periodica polytechnica

Mechanical Engineering
52/2 (2008) 71–76
doi: 10.3311/pp.me.2008-2.06
web: http://www.pp.bme.hu/me

RESEARCH ARTICLE

Measuring the effects of some laser parameters on the surface and near surface region of laser treated cast iron cylinder bore

Kornél Májlinger / *J. Péter* Szabó
Received 2008-10-17

Abstract

The environmental and polluting materials emission standards in Europe are going to be always stricter, so in order to keep up with them, one of the largest European automotive manufacturers performs a laser treatment on the cylinder bores of their combustion engines. In this article the laser treated layers of cast iron cylinder bores with lamellar graphite are investigated with a FISCHERSCOPE® HM2000 XY microhardness measurement system and with a FEI Nova Nanolab 600 SEM/FIB dual beam scanning electron microscope (SEM), equipped with focused Ga-ion beam source. Four samples treated by two different laser sources in three configurations were investigated.

Keywords

laser treatment · cast iron · cylinder bore · microhardness · FIB

Acknowledgement

The authors want to thank the 2. Institute of Physics of the University of Göttingen, where the focused ion beam investigations and the microhardness measurements were made. Additionally thanks to the University of Saarbrücken where the FIB images of Figs. 7-10 were taken. Furthermore thanks for the support of Hungarian Scientific Research Fund (OTKA T 048895). Péter J. Szabó is grateful for the MTA Bolyai János Scholarship.

Kornél Májlinger

Department of Materials Science and Engineering, BME, H–1111 Budapest, Goldmann György tér 3., Hungary
e-mail: pmgpwo@hotmail.com

J. Péter Szabó

Department of Materials Science and Engineering, BME, H–1111 Budapest, Goldmann György tér 3., Hungary
e-mail: szpj@eik.bme.hu

1 Introduction

The automotive engine development is defined by three main factors: first of all there is the need to make the engines more cost effective, the second is that the environmental regulations are becoming stricter, and thirdly the fuel prices are becoming more expensive. The economical requirement of the customers is that even by higher engine power the fuel and oil consumption should not increase, and beside this, engines should have a long lifetime. According to these requirements the main development trends are: reduction of the oil and fuel consumption and longer engine lifetime [1].

Both the consumption reduction and the power increase of Otto- or diesel-engines cause higher pressures in the combustion space. The higher pressure forces the piston rings to the piston bore with higher pressure which results in higher tribological load and therefore in higher wear rate for both components [1]. Increased wear reduces the lifetime of the engines and the gas and oil sealings between piston ring and piston bore become worse. This results in higher oil consumption and higher exhaust, which causes higher emission of pollution materials, decreasing efficiency and decreased engine lifetime.

To improve mechanical and tribological properties of cast iron cylinder bores it is possible to use special mechanical [2] and laser structuring treatments [3], or – as a large European automotive manufacturer uses – a special laser treatment on the V-block engines to alter the properties of the cylinder bores. Due to the laser treatment, the near surface area of the cylinder bore becomes harder and more wear resistant, furthermore, due to the inhomogenity of the perlitic matrix and carbon lamellae, oil reserving holes are formend. This treatment results in an increased power output and a reduced oil consumption [1, 4].

2 The laser treatment

The material of the engines is cast iron with lamellar graphite. The goal of the laser treatment is to melt a thin layer on the surface and at the same time the laser induced plasma over the surface evaporates the graphite lamellas, deeper than the metallic surface itself. So these “holes” are practically non-communicating oil reserves [1]. This treatment is patented, the

patent number is: EP 1 738 859 A1. Recently the cylinder bores in the mass-production are treated with an Xe-Cl excimer laser (Lambda Steel 1000) which works in the UV region, its wavelength is 308 nm at a repetition rate of 300Hz. The maximum stabilized laser output power of the system is over 900W. During treatment the workpiece is treated with a rectangular 3,4×6,4 mm laserspot with 4 times overlap in a definite raster. The adjustable parameters during the laser treatment are:

- scale of the overlap – scanning grid,
- mean laserpower on the surface,
- and the speed of the scanning.

There are further experiments to find alternative laser sources, because the excimer lasers have high maintenance requirements and the maintenance and servicing costs are higher than those of the solid states lasers. A further disadvantage of the currently applied excimer laser is that because of the geometry of the optical output system during laser treatment, the whole cylinder block has to be rotated around the laser output window which significantly reduces the efficiency of the laser system. Furthermore, excimer lasers have large space requirements also.

In this article the results of microhardness mesauremet and the Focused Ion Beam (FIB) study of four samples, treated with Nd-YAG laser and fiber laser sources in three different configurations, will be discussed. The material of the samples is grey cast iron with lamellar graphite (GJL-250). The main laser parameters for the laser treatment are shown in Table 1.

Tab. 1. Main laser parameters for the laser treatment

Sample	Lasering strategy	Laser type	Wavelength	Pulse duratation	Repetition frequecy	Energy density on the surface
A	1×4	Nd-YAG	1064 nm	40 ns	6000 Hz	52 mJ/mm^2
B	2×2	Nd-YAG	1064 nm	40 ns	6000 Hz	52 mJ/mm^2
C	2×2	Nd-YAG	1064 nm	160 ns	6000 Hz	50 mJ/mm^2
D	2×2	Fiber laser	1065 nm	140 ns	12500 Hz	49 mJ/mm^2

The only difference between sample A and B is just in the lasering strategy; sample A was treated with four times overlap of the laser spot (four laser pulses) during the insertion of the laser output tube into the cylinder bore. The samples B, C and D were treated with two times overlap during the insertion as well as during removal (also four laser pulses).

3 Microhardness measurement

The border between macro and micro hardness measurement is 2N, that is, the force is the limiting quantity. Between micro and nano-hardness measurement the border is 0,2 μm in indentation depth, that is, the indentation depth is the limiting factor. In this work micro hardness measurements were performed.

The hardness profile of the surface and the near surface layer of the laser treated surface were measured with a FISCHERSCOPE® HM2000 XY microhardness measurement system which utilized the load-indentation depth method according to ISO 14577-1. The indenter was equipped with a Vickers pyramid. The measuring system was equipped with a microscope too, by which the exact position of the measuring point could be determined. The pyramid was continuously pressed into the material with an increasing test load (load resolution $\leq$ 0.04 mN) and then removed (Fig. 1). The respective indentation depth was measured at the same time, with a distance resolution less than 100 pm [5].

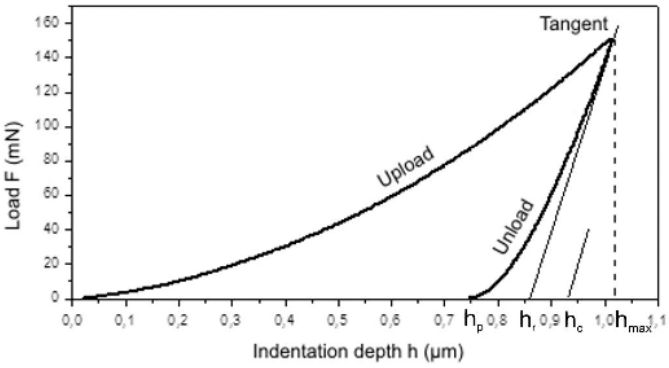

Fig. 1. Load-indentation curve of sample A

By one single measurement information can be obtained about the hardness of the surface, about the hardness pattern within boundary layers near the surface, and about some elastic and plastic properties of the material. The modulus of indentation and the elastic-plastic energy portions can be computed from the recorded measurement plot too [5].

The following measurable characteristic material quantities can be computed according to the standard ISO 14577-1 from the measured data [5]-[6]:

Martens hardness HM: $HM = \frac{F}{A_S(h)}$, where A_S(h) is the cross-section of the diamond pyramid in depth h. It is important to note that the measured penetration of the diamond has an elastic component too, because h=h$_c$+h$_e$, where h$_c$ is the plastic and h$_e$ the elastic component of the indentation.

Indentation hardness H$_{IT}$ *(convertible to HV), s*uitable to describe the plastic behavior of the materials during indentation: $H_{IT} = \frac{F_{\max}}{A_P(h_c)}$, where $S = \left(\frac{dF}{dh}\right)_{h=h\,\max}$is the initial tangent by unload and $h_c = h_{\max} - \frac{\varepsilon \cdot F_{\max}}{S}$. $\varepsilon = 0,75$ for both Vickers- and Berkovich pyramid.

Modulus of indentation

E$_{IT}$:$E_{IT} = (1 - \nu_S^2)\left(\frac{2\sqrt{A_P(h_c)}}{S\cdot\sqrt{\pi}} - \frac{(1-\nu_i^2)}{E_i}\right)^{-1}$.

The modulus of indentation describes (with S initial tangent) the elastic behavior of the materials during indentation. It has a correlation to the E modulus but is not the same. E$_i$ is the elastic modulus of the indentations pyramid and υ_s, υ_i are the Poisson numbers of the probe and the indentations pyramid.

- Elastic component of the indentation work expressed in percent $\eta_{IT} = \frac{W_{elast}}{W_{total}} \times 100$.
- Quantities such as the Martens hardness at a certain test load,

portion of plastic deformation and additional characteristic material quantities according to standards.

The hardness measurements were performed on the laser treated surface. Approximately 10x10 mm size samples were cut out with a precision saw from the engine blocks from the cylinder bore and after smoothing of the back side of the samples they were cleaned in ultrasonic bath. After that, samples were mounted on the table of the microhardness measurement equipment. The main parameters for the microhardness measurement are shown in Table 2.

Tab. 2. Main parameters for the microhardness measurement

Load	Load build up time	Creep time	$h_{max.}$
150 (mN)	40 (s)	5 (s)	1.4 (μm)

4 Focused Ion Beam investigation

The Focused Ion Beam investigations were made by a FEI Nova Nanolab 600 SEM/FIB dual beam scanning electron microscope. This is a combination of a scanning electron microscope and a Ga-ion beam source, and it is capable to machine structures less then 100 nm size and usable for prototyping and analysis. It combines the very high resolution of the electron microscope with field emission cathode and the etching, ion deposition and ion evaporation abilities of a focused ion beam source. With this equipment it is possible to image the surface of the specimen either with the electron or with the ion beam [8]. Within the chamber of the microscope there is a gas injection system. Through its needle it is possible to inject various gases to the surface of the samples from a couple of microns distance. With the various gases it is possible to increase the etching efficiency or to deposit various metals (Pt, W) or insulating layers (SiO_2) on the surface of the sample [8].

A five-step investigation was performed as follows:

Step 1.: First ca. 10x10 mm size samples were cut out with a precision saw from the engine blocks from the cylinder bore and after alignment of the back side of samples they were cleaned in ultrasonic bath and mounted with conductive silver paint on aluminium sample holders.

Step 2.: Through the gas injector system, Pt were injected and deposited first on the surface of the sample in a 20×3 μm quadratic area. The first ca. 100 nm were deposited with the electron beam (Fig. 2) to preserve the near surface layer of the sample from the ion beam induced damage of the Ga-ion beam source [9]. After the electron beam deposition, Pt was deposited with the ion beam source to a thickness of ca. 1 μm (Fig. 3). In this machine the angle between electron beam source and ion beam source is a certain angle so during machining with the ion beam source the samples had to be rotated by 52^o to the electron beam axis.

Step 3.: Along the Pt-layer a stepped cavity were made with Ga- ion bombardement, see Fig. 4a. This process is called "regular cross sectioning". The Pt-layer is needed because otherwise the edge of the sample slightly rounds up – similarly to the normal metallografic sample preparations – so this effect takes place in the Pt-layer. In case of TEM sample preparation the presence of the Pt-layer is needed for further manipulation of the specimen.

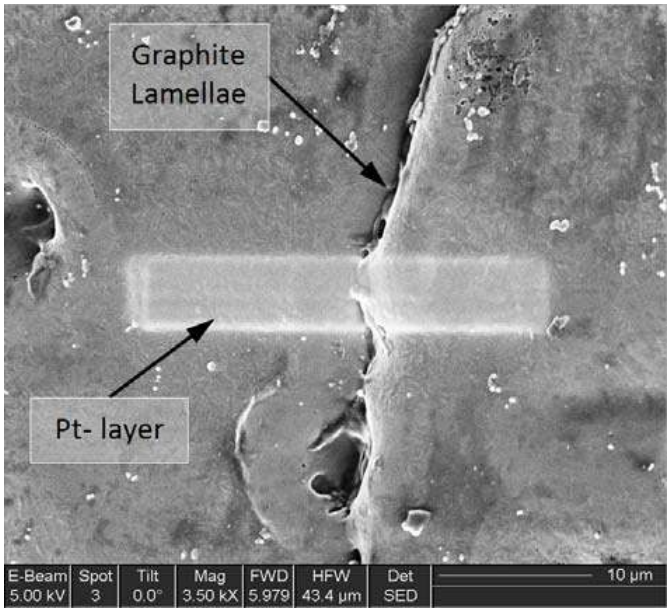

Fig. 2. Electron beam deposited Pt- layer on the non-tilted surface

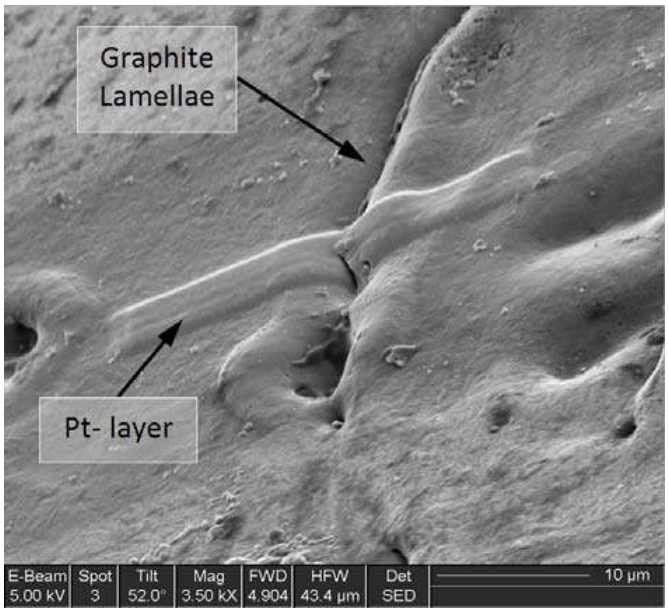

Fig. 3. Ga-ion beam deposited Pt- layer on the tilted surface

Step 4.: Along the long wall of the cavity a further cut was made with lowered ion current (Fig. 4b). This process is called "cleaning cross sectioning".

Step 5.: The surface of that cavity were "etched" with ion beam scanning, and then images were taken with the Ga-ion beam source (Fig. 5). It should be noted that due to the 52° angle between Ga-ion beam and electron beam source, the scale bar applied for the ion beam images is valid only in horizontal direction, while in vertical direction a correction has to be made.

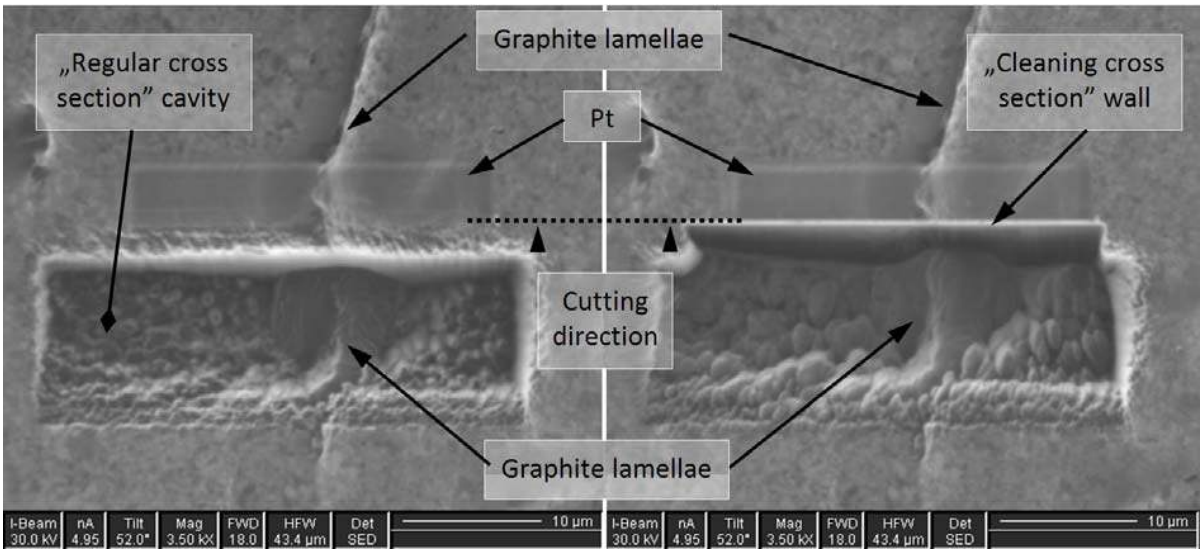

Fig. 4. The cavity – made with Ga- ion bombardement – with graphit lamellae under the surface

The wall of the cavity – made with Ga- ion bombardement – after "cleaning cross sectioning"

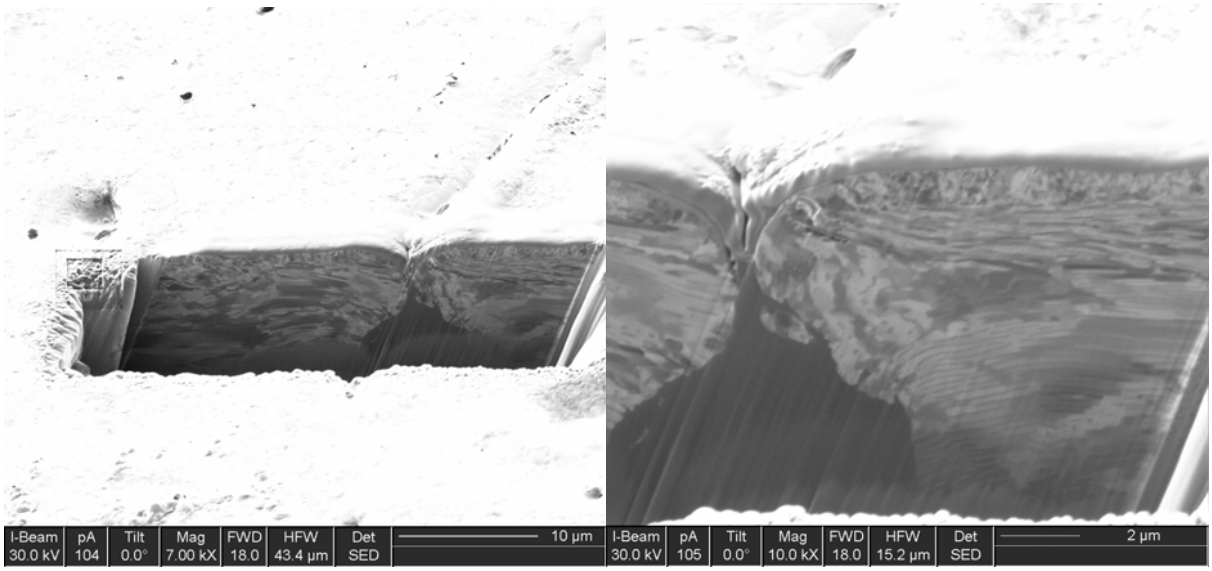

Fig. 5. a. Ga-ion image of the wall of a cavity made by ion-beamb. Ga-ion image of the wall of a cavity made by ion-beam; larger magnification

(It must be noted that in every scanning process by an ion beam during imaging a thin layer of the surface was removed.)

The main parameters for the further focused ion beam investigations (presented later) are listed in Table 3.

Tab. 3. Main parameters for focused ion beam investigations

FIB operation	Accelerator voltage	Ion beam current
Regular cross sectioning	30 kV	3 nA
Cleaning cross sectioning	30 kV	300 pA
Ion beam etching	30 kV	30 pA
Ion beam imaging	30 kV	10 pA

5 Results

Microhardness measurements

Fig. 6 shows the hardness *vs.* indentation depth curves of the four samples. Every curve is the mean value of seven separate measured curves on the same sample. The curves start at 0,1 μm indentation depth, because at the first 100 nm of the indentation – most likely because of the surface roughness of the treted surface – curves have a standard deviation of many order of magnitude. The standard deviation of the mean curves (for every sample) is approx. $\pm$ 500 N/mm^2.

The hardness profiles obtained by 150 mN load (Fig. 6) show that sample A was much harder than the other samples till 400 nm of depth. The hardness values decrease continuously till that, then tend to the value of appox. 3700 HM. Samples B and D are actually very similar, the "softest" hardness profile was obtained for sample C.

The rapid decrease of the hardness from the surface is not surprising, because it will be seen that the laser treated layer is very thin, about 1 μm thick.

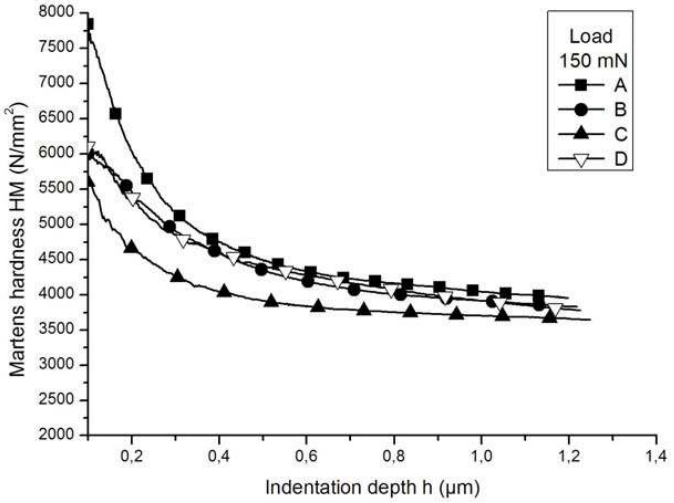

Fig. 6. Hardness profiles obtained by 150 mN load

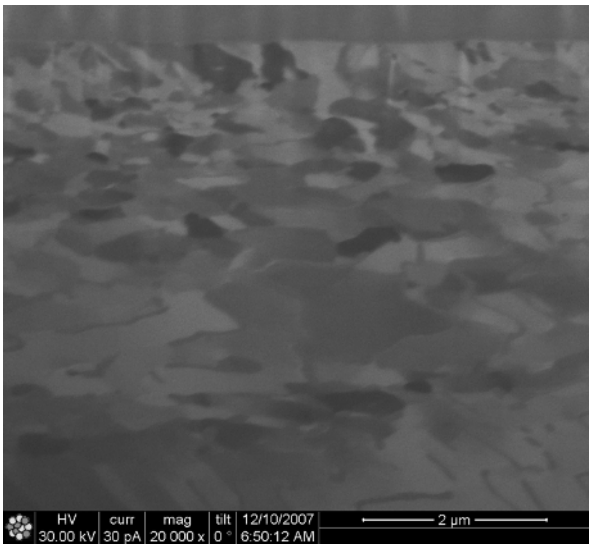

Fig. 7. FIB image (made by ion beam) of the cross section of sample „A"

5.1 FIB investigations

On the FIB cross section images taken by the five-step method described above (Figs. 7-10) it is well seen that the laser treated layer of the pearlitic cast iron is ultra fine grained. Below this layer the base material has many larger grains. The grains of the base material are slightly curved in one direction due to the mechanical machining (milling, bore and honing) of the cylinder bores. The ultra-fine grained structure was most likely formed because of the large heat gradient during solidification of the molten surface.

Tab. 4. The Martens hardness values at 100 nm indentation depth, measured by 150 mN load

Sample	HM_{150mN} (N/mm^2)
A	7700
B	6000
C	5700
D	6200

To determine the average grain size several FIB images were merged together with Corel Draw software, so the merged images covered an area of approx. 20 x 7 μm (20 μm in horizontal and 7 μm in vertical direction). The average grain size was determined along 3 lines. With Image Pro Plus program 3 horizontal lines were drawn into the laser treated layer – from grain boundary to grain boundary – and the number of the grains along these lines with known length were counted. So the grain size is: $d_i = \frac{l_i}{n_i}$, where l_i is the length of the actual line and $n_i$is the number of grains along this line. Therefrom the average grain size is the mean value of the three grain sizes: $\overline{d} = \frac{\sum d_i}{i}$. The average grain sizes and the maximal and minimal values of grain sizes (d_{TEM}) measured by TEM images are listed in Table 5.

The thickness of the laser treated layers on the FIB images was determined with Image Pro Plus image analysis software. The thickness values were measured also by SEM on cross sec-

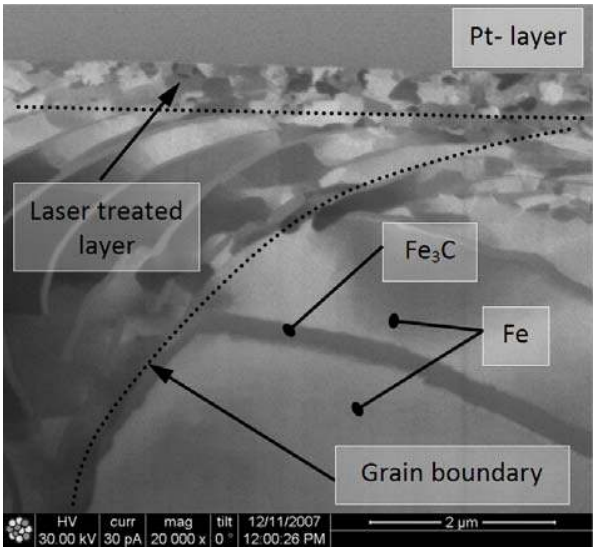

Fig. 8. FIB image (made by ion beam) of the cross section of sample „B"

Tab. 5. Grain sizes of the laser treated layer measured on FIB and TEM images

Sample	$\overline{d}_{FIB}$ (nm)	d_{TEM} (nm)
A	386	150-560
B	179	160-360
C	222	100-400
D	250	—

Tab. 6. The thickness of the laser treated layer of the cylinder bores measured on R_{FIB} -FIB, R_{SEM}-SEM and R_{TEM} - TEM- images

Sample	Laser treated layer thickness		
	R_{FIB} (μm)	R_{SEM} (μm)	R_{TEM} (μm)
A	0.76 - 0.93	0.52 - 1.26	—
B	0.65 - 0.71	0.57 - 1.01	0.5
C	0.85 - 1.18	0.65 - 1.19	1.1
D	0.53 - 1.00	—	0.5 - 0.8

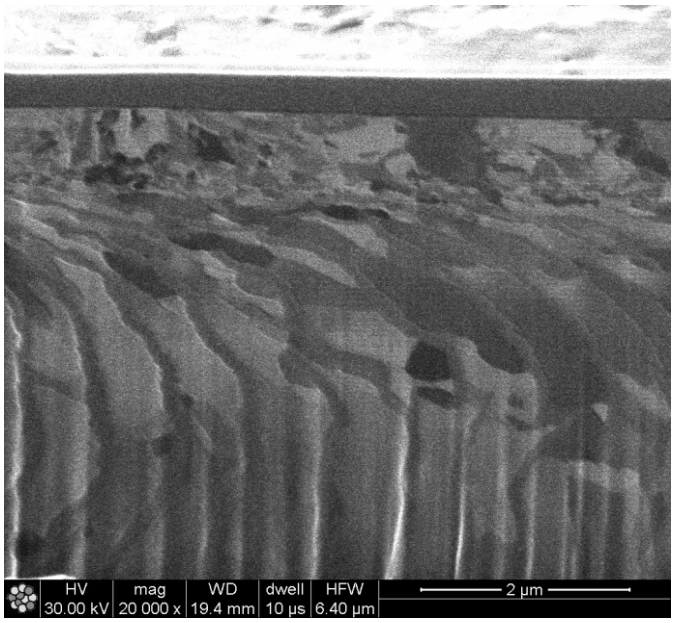

Fig. 9. FIB image (made by ion beam) of the cross section of sample „C"

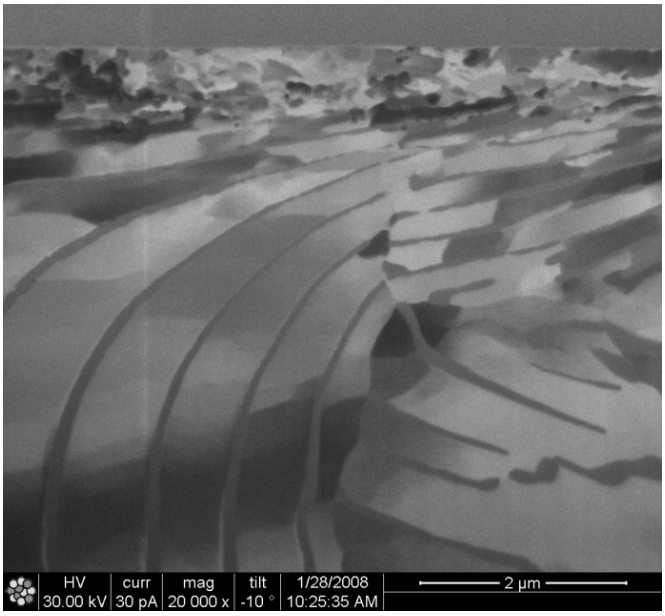

Fig. 10. FIB image (made by ion beam) of the cross section of sample „D"

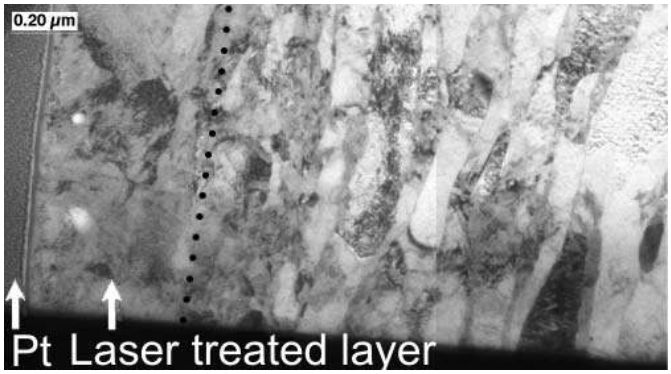

Fig. 11. TEM image of the laser treated surface of sample C and the mechanically heavily deformed near surface layer

tion of the samples prepared by conventional metallographic methods, and by TEM on samples pre-prepared by FIB (see Fig. 11). The layer thicknesses obtained by different methods are listed in Table 6.

6 Conclusions

The hardness measurement curves prone that the surface of the cylinder bores in every case became harder than the base material because of the laser treatment. The hardest surface was observed by the sample **A** which was treated with the short 40 ns laser pulses and with 1x4 time overlap laser strategy. The less hard surface and the thickest laser treated layer were observed by the sample **C** which was probably caused by the longest 160 ns laser pulses.

A possible cause of the increased hardness of the surface and near surface region of the samples is the ultra fine grain size, but the hardness increment is not proportional to the measured hardness values. For identifying the cause of the hardness increment, XRD measurements are planned to be performed, in order to determine the dislocations density and phase composition of the surface and of near surface region.

References

1 **Lindner H, Bergmann H W, Brandenstein C, Lang R, Queitsch A, Reichstein S, Stengel E**, *UV-Laserbelichtung von Grauguß-Zylinderlaufbahnen von Verbrennungskraftmaschienen*, VDI-Berichte (2003), no. 1764, 73-96.

2 **Knoll G, Lagemann V, Lechtape-Grüter R, Robota A, Schlerege F**, *Beeinflussung des Ölverbrauchs von Verbrennungskraftmaschienen durch die Mikrohydrodynamik strukturierter Zylinderoberflächen*, VDI-Berichte (2003), no. 1764, 63-72.

3 **Andersson P, Koskinen J, Varjus S, Gerbig Y, Haefke H, Georgiou S, Zhmudd B, Buss W**, *Microlubrication effect by laser-textured steel surfaces*, Wear **262** (2007), 369–379, DOI 10.1016/j.wear.2006.06.003.

4 **Herbst L, Lindner H, Heglin M, Hoult T**, *Targeting diesel engine efficiency, Industrial Laser Solutions for manufacturing*, 2008.04.04, available at `http://www.helmut-fischer.com/globalfiles/DE_HM2000_PICO_DE.pdf`. Application report.

5 2008.06.08, available at `http://www.dgm.de/past/2004/werkstoffpruefung/download/687_34.pdf`.

6 **Gubicza J, Juhász A**, *Mechanikai tulajdonságok meghatározása mélységérzékeny Vickers keménységmérés módszerével*, Bányászati és kohászati Lapok **8-9** (1997), 315-318.

7 2008.04.10, available at `http://www.nanoscience.hu/education/anyagtudomany/08_pasztazo.pdf`.

8 2008. 05.18, available at `http://www.fei.com/uploadedFiles/Documents/Content/2006_06_Nova600NanoLab_pb.pdf`.

9 **Kwong W. Y, Zhang W. Y**, *Electron beam assisted platinum deposition as a protective layer for FIB and TEM applications*, IEEE 0-7803-9144-06/05, posted on 2005, DOI 10.1109/ISSM.2005.1513408, (to appear in print).

10 **Duffet G, Sallamand P, Vannes A B**, *Improvement in friction by cw Nd:YAG laser surface treatment on cast iron cylinder bore*, Applied Surface Science **205** (2003), 289-296, DOI 10.1016/S0169-4332(02)01119-4.